Characterization of Microgravity Effects on Bone Structure and Strength using Fractal Analysis

Raj S. Acharya, Ph.D.
Director, Biomedical Imaging Group
State University of New york at Buffalo
Buffalo, NY 14260
Phone: (716) 645-2318
email: acharya@eng.buffalo.edu
Date submitted: Oct 12, 94

Linda Shackelford, M.D.
Technical Lead, Bone and Muscle Lab
NASA Johnson Space Center
Houston, Texas 77058
Phone: (713) 483-7100
Fax: (713) 483 6227

Abstract

The effect of micro-gravity on the musculoskeletal system has been well studied. Significant changes in bone and muscle have been shown after long term space flight. Similar changes have been demonstrated due to bed rest. Bone demineralization is particularly profound in weight bearing bones. Much of the current techniques to monitor bone condition use bone mass measurements. However bone mass measurements are not reliable to distinguish Osteoporotic and Normal subjects. It has been shown that the overlap between normals and osteoporosis is found for all of the bone mass measurement technologies: single and dual photon absorptiometry, quantitative computed tomography and direct measurement of bone area/volume on biopsy as well as radiogrammetry. A similar discordance is noted in the fact that it has not been regularly possible to find the expected correlation between severity of osteoporosis and degree of bone loss.

Structural parameters such as trabecular connectivity have been proposed as features for assessing bone conditions. In this report, we use fractal analysis to characterize bone structure. We show that the fractal dimension computed with MRI images and X-Ray images of the patella are the same. Preliminary experimental results show that the fractal dimension computed from MRI images of vertebra of human subjects before bedrest is higher than during bedrest.

1 Introduction

The effect of micro-gravity on the musculoskeletal system has been well studied. Significant changes in bone and muscle have been shown after long term space flight. Similar changes have been demonstrated due to bed rest. Bone demineralization is particularly profound in weight bearing bones. Much of the current techniques to monitor bone condition use bone mass measurements. However bone mass measurements are not reliable to distinguish Osteoporotic and Normal subjects [29]. It has been shown that the overlap between normals and osteoporosis is found for all of the bone mass measurement technologies: single and dual photon absorptiometry, quantitative computed tomography and direct measurement of bone area/volume on biopsy as well as radiogrammetry. A similar discordance is noted in the fact that it has not been regularly possible to find the expected correlation between severity of osteoporosis and degree of bone loss [30].

Structural parameters such as trabecular connectivity have been proposed as features for assessing bone conditions [29]. It has been shown that in vertebral crush fracture patients, elements such as vertical trabeculae are retained more or less intact, while elements such as horizontal bracing trabeculae are resorbed entirely [31] [32] . This results in disconnection of large number of trabecular elements. However, in non-fracture patients connections between elements were preserved. Long vertical trabeculae are subject to buckling under loading. When they lose their lateral connections to adjacent trabeculae, the degree of buckling may exceed the inherent strength of the bone. Structure can be thus be seen as an important feature in assessing bone condition.

2 Significance

Protecting humans against extreme environmental conditions requires a thorough understanding of the pathophysiological changes resulting from the exposure to those extreme conditions. The knowledge of the degree of medical risk associated with the exposure is of paramount importance in the design of effective prophylactic and therapeutic measures for space exploration. Major health hazards due to musculoskeletal systems include the signs and symptoms of hypercalciuria, lengthy recovery of lost bone tissue after flight, possibility of irreversible trabecular bone loss, the possible effect of calcification in the soft tissues, and the possible increase in fracture potential. Our research to relate the local trabecular structural information to microgravity conditions is an important initial step in understanding the effect of microgravity and countermeasures on bone condition and strength. The proposed research is also closly linked with Osteoporosis and will benefit the general population.

3 Hypothesis/Rationale

- The rationale for this research is based on the premise that microgravity conditions change bone structure as well as bone mass.
- Bone structure can be characterized by fractal geometry.

- Fractal characterization of bone structural changes due to microgravity conditions is not only optimal but also pragmatic.

4 Specific Tasks Achieved

The overall goal is the characterization of bone structural changes due to microgravity with the aid of fractals.

- We have related the fractal dimension computed from MRI images to those obtained with X-Rays of the same specimen.
- We have computed the fractal dimension from MRI images of subjects before, during and after bed rest.
- We have computed the fractal dimension of faxitron images of Osteoporotic and Normal Bone slices of human subjects.

During the summer fellowship, we have implemented and tested the fractal algorithms on sample MRI bone images.

The long term goal we are pursuing is to integrate fractal and finite element analysis. We are interested in studying the effect of various external parameters on local structural information provided by our method. This makes it possible to quantify the effect of countermeasures on local structural information of the bones.

5 Summary of Results Achieved

- Fractal Dimension of the human subject tested is higher before bedrest than during bedrest. This shows that the Fractal Dimension decreases due to bedrest.
- Fractal Dimension of Osteoporotic subjects is less than the Fractal Dimension of Normal Subjects in the Faxitron Image Study.
- Fractal Dimension measured with the MRI image and X-Ray image of the Patella is the same.

6 Fractal Model

With natural objects, familiar metrics from classical geometry such as *length, area* and *volume* depend on the scale at which we decide to look at the object (*e.g.* the size of the "yard stick"). As an example, one can show that the surface area of a sand grain is entirely dependent on the scale at which one chooses to look at it. The smaller the scale, higher the surface area since more nooks and crannies become visible.

Fractal geometry [12] characterizes this ability of an n dimensional object to fill the $n+1$ dimensional space where the relationship of a measure M with topological dimension n and the scale ϵ is expressed as

$$M(\epsilon) \propto \frac{1}{\epsilon^r}, \quad 0 \leq r \leq 1 \tag{1}$$

where the quantity $r + n$ (denoted by D) is called the *fractal dimension* or *Hausdorf-Besicovich dimension* and characterizes the degree of erratic behavior. For an ideal object, the measure M is independent of the scale ϵ and hence $n = D$. Thus a fractal object can be defined as a set for which the fractal dimension is greater than the topological dimension. There are number of ways in which fractal geometry can be applied to the analysis of texture in images. Pentland et.al [19] used a method related to the cooccurance matrix technique of texture classification based on fractal dimension. They find the standard deviations of the difference of gray levels separated by a given vector and plot it against the vector lengths as a log-log graph. In another technique [18] two dimensional gray level image is represented as a three-dimensional surface whose height at each point represents the gray level at that point and the surface area is measured at different scales. It has also been shown that [9] a n-dimensional fractal object can be characterized by the fractional Brownian motion of n variables and that the relationship between the power spectral density and r are independent of the projection [7]. This makes the fractal dimension computed from the projections of n-dimensional fractal object represent that of the original object.

It has been shown that the power spectra of a fractal object exhibits an inverse-power relation to frequency. For one-dimensional signals, this can be expressed as,

$$S(\omega) \propto \frac{1}{|\omega|^r} \tag{2}$$

and the parameter r is related to the fractal dimension by the equation,

$$D = \frac{5 - r}{2} \tag{3}$$

Thus one can exploit the above relationships to estimate the fractal dimension in frequency domain by finding the slope of the plot of log power spectra vs. log frequency. For multi-dimensional case, the corresponding relationship has been shown to be

$$S(\omega_1, \omega_2, \cdots, \omega_n) \propto \frac{1}{(\omega_1^2, \omega_2^2, \cdots, \omega_n^2)^{\frac{r}{2}}} \tag{4}$$

where

$$D = \frac{2n + 3 - r}{2} \tag{5}$$

In the next section, we reiterate some basic morphological operations and present an algorithm to obtain the fractal dimension of a three dimensional surface. This approach gives us the added capability of dealing with shape using different structuring elements. Since the underlying theme is based on fractals, all of the above properties hold for morphological fractals as well.

Our approach is based on the above method where the digitized radiograph is represented as a surface whose height represents the gray level at each point. The surface area at different scales is estimated using a series of dilations of this surface by a given structuring element whose size determines the scale. The derivations in the next section shows how one can obtain the surface area from the volume of the dilates and some simplifications which allows one to use dilations by a fixed size structuring element.

7 MORPHOLOGICAL FRACTALS

Mathematical Morphology as developed by Matheron and Serra [25] is basically a Set Theory and uses set transformations for Image Analysis. It extracts the impact of a particular shape on images via the concept of Structuring Element (SE). The SE encodes the primitive shape information. In a discrete approach, the shape is described as a set of vectors with respect to a particular point, the Center, which does not necessarily belong to the SE. During Morphological transformation, the Center scans the whole image and matching shape information is used to define the transformation. The transformed image is thus a function of the SE distribution in the original image.

In particular, *Dilation* of a set X with a SE Y is given by the expression

$$X \oplus Y = \{x : Y^x \cup X \neq \emptyset\} \tag{6}$$

where Y^x indicates the translation of set Y with x. The operations gives a set whose surface is the path traced by the center of the SE Y when it traverses along the surface of X. Using the above operation, surface area of a compact set X with respect to a compact convex SE Y which is symmetrical with respect to the origin is given by [25] :

$$S(X,Y) = \lim_{\rho \to 0} \frac{V(\partial X \oplus \rho Y)}{2\rho} \tag{7}$$

where ∂X is the boundary of set X and $\oplus$ denotes the dilation of the boundary of set X by the SE Y scaled by a factor ρ. $V(X)$ gives the volume of set X It has been observed that even though for "regular" classes of sets, the surface area $S(X,Y)$ is finite, for many "natural" objects, this can be infinite.

From the above expressions, it can be seen that dilating by ρY hides all structures smaller than ρY and therefore is equivalent to looking at the surface at scale ρ. For experimental purposes, we can calculate the surface area of a set X at scale ρ

$$S(\partial X, Y, \rho) = \frac{V(\partial X \oplus \rho Y)}{2\rho} \tag{8}$$

If the object is regular, the surface area will not change with ρ_i. For a fractal object, $S(\partial X, Y, \rho)$ increases exponentially with decreasing ρ as seen from equation (1). By taking the logarithm, we now have

$$\begin{aligned} \log\left(S(\partial X, Y, \rho)\right) &= \log(K) - r\log(\rho) \\ D &= 2 + r \end{aligned} \tag{9}$$

Where K is the proportionality constant. We can now estimate D by plotting $\log[S(\partial X, Y, \rho_i)]$ Vs. $\log[\rho_i]$ for a given set of scale factors ρ_i, $i = 1, 2, \cdots, N$ and calculating the gradient of the line that fits the plot.

The series of dilation of X by $\rho_i Y$ required for the above computation can be further reduced to dilation by the unit element Y by observing that if $X_Y^\rho = X \oplus \rho Y$, then

$$X_Y^{\rho+1} = X \oplus (\rho + 1)Y = (X \oplus \rho Y) \oplus Y = X_B^\rho \oplus Y \tag{10}$$

Apart from having projection angle and scale invariance, with the morphology method, we also have the freedom of selecting a structuring element suited for the problem at hand. This, coupled with the fact that the method only involves dilation makes the implementation straightforward compared with the other methods where it is required to find the covering of the boundary of X (∂X) by spheres in 3D and disks in 2D.

The surface area $S(X, Y, \rho_i)$ can be iteratively calculated as follows: Let the image X be defined as the set of triplets $\{< f(x, y); x = 1, N; y = 1, M\}$ and the the structuring element Y be given as a set of triplets $\{< x_i, y_i, z_i >,\ i = 1, P\}$. The ρ^{th} dilate $f_\rho(x, y)$ is calculated as

$$f_\rho(x, y) = \max\{f_{\rho-1}(x + x_i, y + y_i) + z_i,\ i = 1, 2, \cdots, P\} \tag{11}$$

The initial condition $f_0(x, y)$ is set to $f(x, y)$.

The surface area at each step can be calculated by using equation(8) where

$$S(X, Y, \rho) = \frac{V(X, Y, \rho)}{2\rho} = \frac{\sum_{x \in 1,N; y \in 1,M} (f_\rho(x, y) - f(x, y))}{2\rho} \tag{12}$$

8 Alternating Sequential Filters

In this section we will use Morphological Pyramids to compute the Fractal Dimension. Generally, dilation and erosion are applied in pairs to make the transformation independent of the origin of the SE. The opening operation of a set F by a SE B is defined as,

$$F \circ B = (F \ominus B) \oplus B$$

The dual operation closing is defined as

$$F \bullet B = (F \oplus B) \ominus B$$

A composite opening-closing mapping can be defined as,

$$M_B(F) = (F \circ B) \bullet B$$

An iterative application of such an operator is defined as a Alternating Sequential Filter(ASF) [15],[26].

$$ASF(F) = M_{B_N} M_{B_{N-1}} ... M_{B_1}(F)$$

where N is an integer and $B_N, B_{N-1}, ...B_1$ are SEs with different sizes satisfying the constraint $B_N \supseteq B_{N-1} \supseteq ...B_1$.

During a morphological transformation, the structuring element scans the whole image and modifies each point depending on the structural similarity of the SE with the image at that point. During erosion, any structure in the foreground smaller than the SE is removed from the image. Similarly, dilation removes such structures in the background. The composite operation of opening and closing provides the same result with the added advantage of independence from the origin of the SE. The result of such a transformation can be interpreted as a transformation where the details of the original image smaller than the SE are removed. Thus the repeated application of such transformations using SE with increasing size will result in a sequence of images with decreasing details. This is equivalent to a representation of the image at decreasing resolution. This multiresolution representation is used for the surface area measurement.

Though opening and closing are sufficient for such a purpose, use of ASF is preferred. ASF is more robust and introduces less distortion than individual application of opening or closing [15]. A smaller structuring element should be used before a larger one.

The direct application of ASF needs iterative morphological transformation using increasing structuring elements. As the SE size increases, the computation involves increases. In [15], it has been shown using morphological sampling theorem [4] that ASF pyramid can be obtained equivalently by decreasing the size of the image instead of increasing the size of structuring element. At any level of the pyramid, the next level representation is obtained by subsampling the image and then transforming the sampled image using a constant sized element. As the image size is decreased and the SE size remains unchanged, this process is more efficient.

Once the morphological pyramid is obtained, the surface area is computed using a *piecewise planer* approximation. The image is viewed as a sampled version of continuous two-dimensional surface. In the approximation, the surface is considered as the union of non-overlapping triangular areas. The triangles are formed in two steps. First, the support of the surface is divided into a number of squares, each having the side equal to one grid spacing. An $M \times N$ image is composed of MN such unit squares. Each square is represented by the pixels at four corners $(p,q), (p+1,q), (p,q+1)$ and $(p+1,q+1)$. In the next step, each such square is divided into two triangles, one of which is represented by the pixels at $(p,q), (p+1,q)$ and $(p,q+1)$ and the other by $(p+1,q)$, $(p+1,q+1)$ and $(p,q+1)$. The area of any such triangle is computed using the pixel gray level values of its three corners. The surface area of the image is approximated by the sum of the area of all the triangles. The image size decreases as the resolution decreases. To represent the correct surface area at all resolutions, the area computation takes the resolution step into account by normalizing the grid space (for example, the grid spacing in the 1/4-th resolution represents 4 gridspacing of the original resolution).

The slope of the log-log plot of the surface area against the resolution is computed using least-square estimation.

9 Preliminary Experimental Results

9.1 Relating the Fractal Dimension of X-Ray and MRI images of the patella.

An isolated human patella was scanned in MRI scanner. Additionally, X-Ray images of the same patella was obtained. Fractal dimension was computed in four different regions of the MRI image with a window size of 50. Fractal Dimension was also computed in the same regions on the X-Ray image. Figure 1 shows the MRI image and the X-Ray image of the patella. The computed fractal dimension in each of the four different areas are shown. The tabulated results in figure 1 show that there is no significant difference between the fractal dimension computations between the MRI image and the X-Ray image.

9.2 Faxitron Bone Images of Osteoporotic and Normal Subjects

Faxitron bone images of the normal and human subjects were obtained. Fractal dimension was computed with a window size of 110 by 110 on six slices of normal and 8 slices of osteoporotic bone images. The fractal dimension computed with the flat and pyramid SEs are shown. The fractal dimension computed on the osteoporotic subjects was smaller than the fractal dimension computed with the normal subjects.

9.3 Bedrest Studies

Fractal dimension was computed on a series of MRI images of the vertebra of human subjects scanned before, during and after bedrest. The computed result on figure 3 shows that the fractal dimension of the subject before bedrest was higher than the fractal dimension during bedrest.

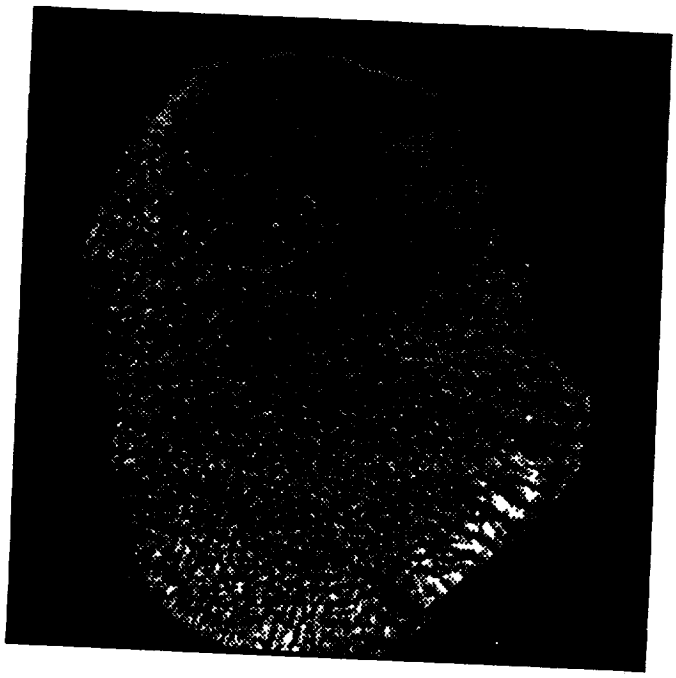

MRI image of patella

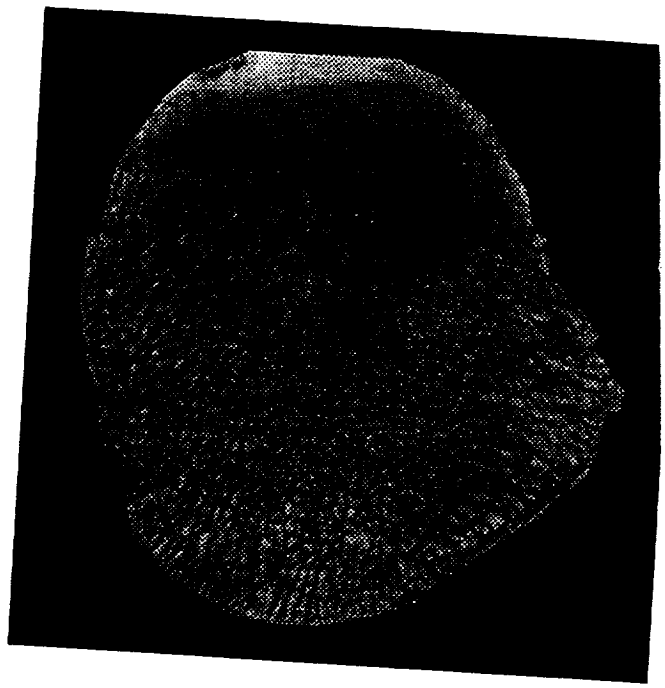

X-Ray image of patella

s/patella_pieces2/MRI-patella.1.	50	D=2.799259
s/patella_pieces2/MRI-patella.2.	50	D=2.797808
s/patella_pieces2/MRI-patella.3.	50	D=2.736876
s/patella_pieces2/MRI-patella.4.	50	D=2.694368

s/patella_pieces2/XRAY_patella.1.	50	D=2.804438
s/patella_pieces2/XRAY_patella.2.	50	D=2.750343
s/patella_pieces2/XRAY_patella.3.	50	D=2.735890
s/patella_pieces2/XRAY_patella.4.	50	D=2.622544

Fig 1: Fractal Dimension of X-Ray and MRI image

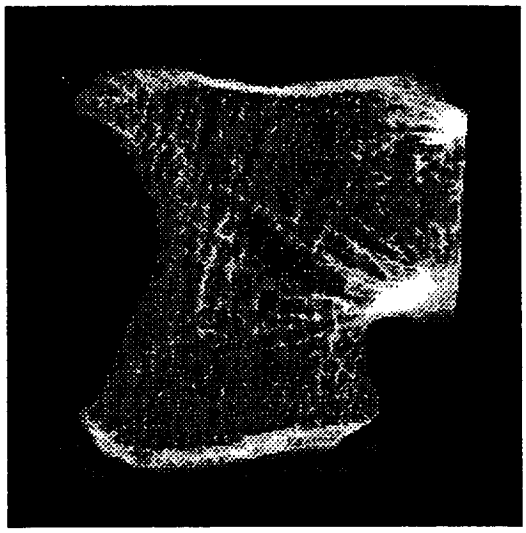

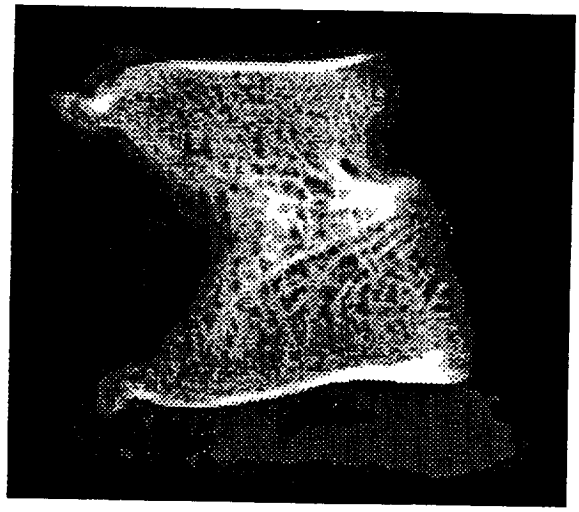

Please note that the fractal number can vary between 2 and 3.
The differences obtained between the groups is quite significant.

/***** Results from 152_L4 stack using morphology *****/
/***** Each region-of-interest is of dim. 110x110 *****/

		Flat	Pyramid	
es/152_L4_1.1.	110	D=2.609848	D=2.543952	
es/152_L4_2.1.	110	D=2.670599	D=2.595224	
es/152_L4_3.1.	110	D=2.661320	D=2.598183	Normal
es/152_L4_4.1.	110	D=2.667757	D=2.597461	
es/152_L4_5.1.	110	D=2.667157	D=2.593838	
es/152_L4_6.1.	110	D=2.674416	D=2.610721	

/***** Results from 16_L4 stack using morphology *****/
/***** Each region-of-interest is of dim. 110x110 *****/

s/16_L4_2.1.	110	D=2.478800	D=2.417768	
s/16_L4_3.1.	110	D=2.523201	D=2.451674	
s/16_L4_4.1.	110	D=2.518456	D=2.447915	
s/16_L4_5.1.	110	D=2.514385	D=2.446387	Osteoprotic
s/16_L4_6.1.	110	D=2.572345	D=2.481285	
s/16_L4_7.1.	110	D=2.572345	D=2.481302	
s/16_L4_8.1.	110	D=2.450142	D=2.402326	
s/16_L4_9.1.	110	D=2.482301	D=2.425839	

Fig 2: Fractal Dimension of Normal & Osteoprotic images.

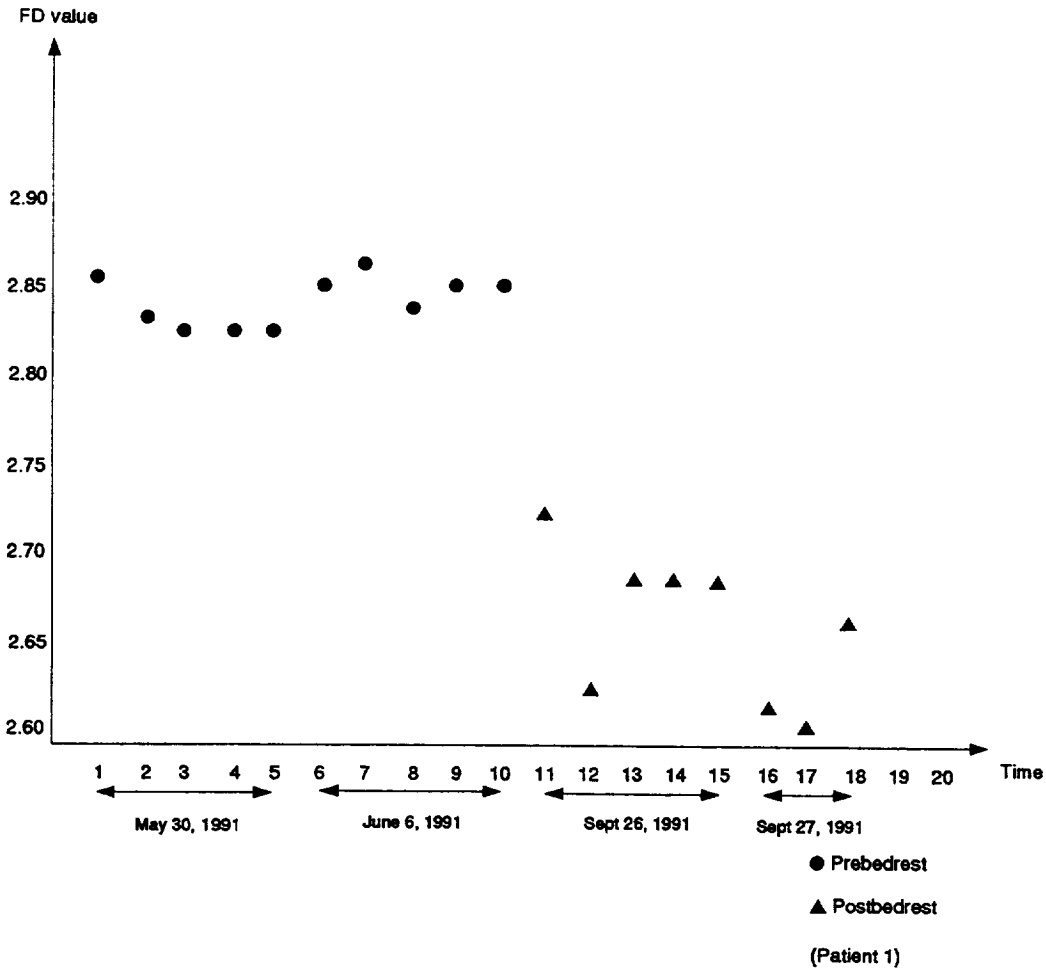

Fig 3: Bedrest Study

10 Conclusion

We use fractal dimension to characterize bone structure. We see that the fractal dimension computed with MRI images and X-Ray images of the patella are the same. We find that the fractal dimension of the Osteoporotic subjects to be less than the fractal dimension of Normal subjects. We also show that the fractal dimension of the subjects during bedrest is less than the fractal dimension before bedrest.

References

[1] C. B. Caldwell and et al. Characterization of Mammographic Parenchymal pattern by Fractal Dimension. *Phys. Med. Biol*, 35, 1990.

[2] R. M. Haralick. Statistical and structural approaches to texture. *Proc. IEEE 67*, pages 786–809, May 1979.

[3] R. M. Haralick and et al. Image Analysis Using Mathematial Morphology. *IEEE Trans. Pattern Anal. Mach. Intelligence*, 9, July 1987.

[4] R. M. Haralick and et al. The Digital Morphological Sampling Theorem. *IEEE Trans. Acous. Speech and Signal Proc.*, 37, December 1989.

[5] E. Hausmann, K. Allen, L. Christersson, and R. Genco. Effect of x-ray beam vertical angulation on radiographic alveolar crest measurement. *J periodontal Res.*, 24:8–19, 1989.

[6] J. Keller and et al. Texture Description and Segmentation Through Fractal Geometry. *Comput. Vision, Graph. Image. Proc.*, 45, 1989.

[7] W. S. Kuklinski, K. Chandra, U. E. Ruttimann, and R. Webber. Application of fractal texture analysis to segmentation of dental radiographs. In *Medical Imaging III: Image Processing*, volume 1092. SPIE, 1989.

[8] S. Y. Lu and K. S. Fu. A syntatic approach to texture analysis. *Computer Graphics and Image Processing*, 7:303–330, 1978.

[9] T. Lundahl, W. J. Ohley, S. M. Kay, and R. Siffert. Fractional brownian motion: A maximum likelihood estimator and it's application to image texture. *IEEE Transactions in Medical Imaging*, MI-5:152–161, Sept. 1986.

[10] A. Lynch and et al. Analysis of texture in Macroradiographs of osteoarthritic knees using fractal signatures. *Phys. Med. Biol.*, 36, 1991.

[11] S. Mallat. A Theory for Multiresolution Signal Decomposition: The Wavelet Representation. *IEEE Trans. Pattern Anal. Mach. Intelligence*, 11, July 1989.

[12] B. B. Mandelbrot. *Fractals: Form, Chance and Dimension.* Freeman, San Fransisco, 1977.

[13] B. B. Mandelbrot. *Fractal Geometry of Nature.* Freeman Press, 1982.

[14] D. Marr. Analyzing natural images: A computational theory of texture vision. *Cold Spring Habor Symposia on Quantitative Biology*, XL:647–662, 1976.

[15] A Morales and R. Acharya. Morphological Pyramids with Alternating Sequential Filters, IEEE Trans on Image Processing (In Press).

[16] T. Pavlidis. A review of argorithms for shape analysis. *Computer Graphics and Image Processing*, 7:243–258, 1978.

[17] S Pelag and et al. Multiple Resolution Texture Analysis. *IEEE Trans. Pattern Anal. Mach. Intelligence.*

[18] S. Peleg, J. Naor, R. Hartley, and D. Avnir. Multiple resolution texture analysis and classification. *IEEE Transactions on Pattern Analysis and Machine Intelligence*, PAMI-6(4):518–523, July 1984.

[19] A. Pentland. Fractal-based description of natural scenes. In *IEEE Computer Society Conference*, Computer Vision and Pattern Recognition, pages 210–209, Washington, DC, June 1983.

[20] A. Rosenfeld. A note on automatic detection of texture gradients. *IEEE Transactions on Computers*, 10:988–991, 1975.

[21] U. Ruttimann and et al. Fractal Dimension from Radiographs of Peridontal Alveolar Bone: A possible Diagnostic Indicator of Osteoporosis.

[22] U. E. Ruttimann and J. A Ship. The use of fractal geometry to quantitate bone structure from radiographs. *J. Dent. Res*, page 69, 1990. Abstract no. 1431.

[23] J Samarabandu and et al. Analysis of BOne X-Rays Using Morphological Fractals. *IEEE Trans. Med. Imag.*, 12:466–70, September 1993.

[24] N. Sarkar and B. B. Chaudhuri. An Efficient Approach to Estimate Fractal Dimension of Texture Images. *Pattern Recog.*, 25, 1992.

[25] J. Serra. *Image Analysis and Mathematical Morphology, vol 1.* Academic Press, 1982.

[26] S. Sternberg. Grey Scale Morphology. *Comput. Vision, Graph. Image. Proc.*, 35, 1986.

[27] H. Voorhees and T. Poggio. Detecting textons and texture boundaries in natural images. In *1st International Conference on Computer Vision*, pages 250–258, London, June 8–11 1987.

[28] R. L. Webber, J. B. Hazelrig, R. J. Patel, H. R Van Den Berg, and J. E. Lemmons. Evaluation of site-specific differences in trabecular bone using fractal geometry. *J. Dent. Res.*, page 70, 1991. Abstract no. 2095.

[29] R. Heaney, "Osteoporotic Fracture Space: An Hypothesis," *Bone and Mineral*, 6(1989), 1-13.

[30] J. Podenphant et al, "Bone mass, bone structure and vertebral fractures in osteoporotic patients," *Bone*, 1987, 8:127-130.

[31] M. Kleerekoper et al, "Cancellous bone architecture and bone strength," *Osteoporosis 1987*, 294-300.

[32] J.E. Aaron et al, "The microanatomy of of trabecular bone loss in normal aging men and women," *Clin Orthop Res*, 1987, 215:260-271.

[33] J. Samarabandu, R. Acharya, E. Hausman, C. Allen, "Analysis of Bone Images using Morphological Fractals", *IEEE Trans on Medical Imaging*, 12, Sep 1993, pp466-470.

4960

N95-32420

Application of Impact Dampers in Vibration Control of Flexible Structures

Final Report
NASA/ASEE Summer Faculty Fellowship Program--1994
Johnson Space Center

Prepared by:	Fred A. Akl, Ph.D. P.E. Aamir S. Butt, M.S.
Academic Rank:	Professor Graduate Student
College and Department:	Louisiana Tech University Department of Civil Engineering Ruston, LA 71272
NASA/JSC	
Directorate:	Engineering
Division:	Structures and Mechanics
Branch:	Loads and Structural Dynamics
JSC Colleague:	David A. Hamilton
Date Submitted:	August 5, 1994
Contract Number:	NGT-44-005-803